# The oxidation state of Ti in hibonite at the atomic scale

Pierre-marie Zanetta[1], Yao-Jen Chang[1], Tarunika Ramprasad[2], Venkat Manga[1], Juliane Weber[3] and Thomas Zega[4]

[1]Lunar and Planetary Laboratory, Tucson, Arizona, United States, [2]Materials Science and Engineering, University of Arizona, Tucson, Arizona, United States, [3]Chemical Sciences Division Oak Ridge National Laboratory, Oak Ridge TN 37830, United States, [4]Lunar and Planetary Laboratory, University of Arizona, United States

A wide range of phases in planetary materials can host *3d* transition metals in multiple oxidation states. Hibonite ($CaAl_{12}O_{19}$) is of particular interest because (i) it is one of the first phases to form at high temperature in the solar nebula [1] and (ii) significant amounts of transition metals such as Ti, V, and Fe were reported in its structure [2, 3]. The Ti in hibonite was shown to occur in both $Ti^{3+}$ and $Ti^{4+}$ oxidation states in hibonite [4, 5]. The exact mechanism of Ti incorporation is debated [6–9], but measurement of its oxidation states can provide information on the thermodynamic conditions (temperature, composition of the gas, oxygen fugacity) under which it formed or last equilibrated. Electron energy-loss spectroscopy (EELS) in the transmission electron microscope (TEM) can obtain information on the oxidation states of *3d* metals in a wide range of materials [10–13]. Several methods were described in the literature. Here we describe a modified white-line method to quantify Ti-oxidation states with application to meteoritic hibonite.

We acquired spectra of Ti-oxide standards of known $Ti^{3+}/Ti^{4+}$ content including TiO ($Ti^{2+}$), $Ti_2O_3$ ($Ti^{3+}$), $Ti_3O_5$ ($Ti^{4+}:Ti^{3+}= 1:2$), $Ti_4O_7$ ($Ti^{4+}:Ti^{3+}= 1:1$), $TiO_2$ ($Ti^{4+}$), $FeTiO_3$ ($Ti^{4+}$), $CaTiO_3$ ($Ti^{4+}$) using a 200 keV aberration-corrected Hitachi HF5000 S/TEM equipped with a Gatan Quantum ER electron energy-loss spectrometer. Spectra were acquired in STEM mode over an ~200 x 200 nm field of view using a 25 µm condenser aperture (probe current ~ 105 pA), a 2.5 mm spectrometer entrance aperture, and a dispersion of 0.025 eV/ch with a dwell time of 0.5 sec/pixel. To improve our understanding of spectral features, we performed first-principle calculations using the Wien2k code and simulated the Ti-oxide spectra via TELNES 3 (Theoretical Electron Energy Loss Near Edge Spectra) [14, 15].

Using the same experimental conditions, we analyzed the $L_{2,3}$ edge of both synthetic and meteoritic hibonite grains prepared using a focused-ion-beam scanning-electron microscope (FIB-SEM). Synthetic hibonite FIB sections were extracted from the ALL sample series reported in [6]. The natural hibonite was extracted from a compact type-A (CTA) calcium-aluminum-rich inclusion (CAI) within the NWA 5028 CR2 chondrite [16]. In addition, we performed atomic-scale EELS spectrum imaging on the hibonite from the CTA of NWA 5028. Such atomic-scale measurements require faster acquisition time to minimize sample drift and carbon deposition. Thus, to improve the EELS signal, we used a 30 µm condenser aperture, (probe current ~150 pA) and a 5 mm spectrometer entrance aperture, providing an EELS collection angle of β=63 mrad. Spectra were acquired using a dispersion of 0.5 eV/channel with a drift tube offset of 300 eV. All spectra were processed using Hyperspy [17].

The spectra from the Ti oxides show a chemical shift of the $L_{2,3}$ edge that correlates with the valence state of the material. Simulated spectra match well to the experimental spectra and confirm the chemical shift (Fig. 1). We tested the white-line ratio method (i.e. $IL_2/IL_3$) based on previous descriptions [10, 12, 13]

to develop a calibration curve for our electron-optical conditions. We obtained an exponential relationship between the $IL_2/IL_3$ ratio and the $Ti^{4+}$ abundance. However, because Ti standards and synthetic hibonite with high $Ti^{4+}/\Sigma Ti$ values ( $>0.8$) display strong ($\pm 50\%$) $IL_2/IL_3$ variations, the fit that we obtained is markedly different than what was previously reported [13]. This discrepancy is due to the edge offset window ($IL_2$). Our TELNES simulations show that the onset position of the Ti $L_{2,3}$ is dependent of the oxidation state, but the position of the offset depends on both the chemical shift and the crystal-field effects due to site geometry. Our results suggest that dependency of the white-line ratio on both effects complicates the development of a reproducible universal curve for Ti. Thus, we explored an alternative approach involving only the chemical shift at edge onset.

We quantified the onset normalized intensity of the $L_3$ edge using a window of 2 eV ranging from 455 to 457 eV. We find that the $L_3$ integrated intensity decreases as a function of increasing oxidation state. This decrease is due to the shift of the onset position which itself is controlled by the width of the band gap that increases with a decreasing number of *d*-electrons. We fit the data to a polynomial function which yields a 0.99 correlation coefficient (Fig 1b).

The obtained calibration was used to quantify the $Ti^{4+}/\Sigma Ti$ ratios of previously synthesized hibonites. $Ti^{4+}/\Sigma Ti$ ratios measured from our approach are 0.91±0.01 (ALL2-6), 0.88±0.01 (ALL2-57), and 0.84±0.01 (ALL2-55), which compare favorably with those ratios of 0.94±0.01, 0.89±0.01, and 0.84±0.01 respectively, measured by [6] using electron spin resonance (ESR) spectroscopy. The agreement of the data sets from these orthogonal approaches suggests that the alternative method works under our optical conditions and can be applied to other samples.

To that end, we tested the method on a meteoritic hibonite grain extracted from a CTA in the NWA 5028 CR2 chondrite and obtained a $Ti^{4+}/\Sigma Ti$ mean value of 0.78±0.01. Additionally, atomic-scale measurements confirmed that Ti occupies the M2 and M4 sites [8, 18]. To determine whether the Ti oxidation state varies spatially within the same grain, we performed EELS spectrum imaging and mapped the $Ti^{4+}/Ti^{3+}$ ratio. We find that the grain contains a $Ti^{4+}/Ti^{3+}$ gradient (over 100 nm) ranging from 1±0.05 to 0.7±0.05 near its boundary with adjacent material. It was suggested that during the formation of CTAs, the condensate assemblages experienced thermal processing [19]. Such processing included partial melting and recrystallization, leading to rounded morphologies and 'compact' inclusions. We infer that the measured $Ti^{4+}/Ti^{3+}$ gradient in the hibonite was recorded during the high-temperature process that affected its host CTA CAI.
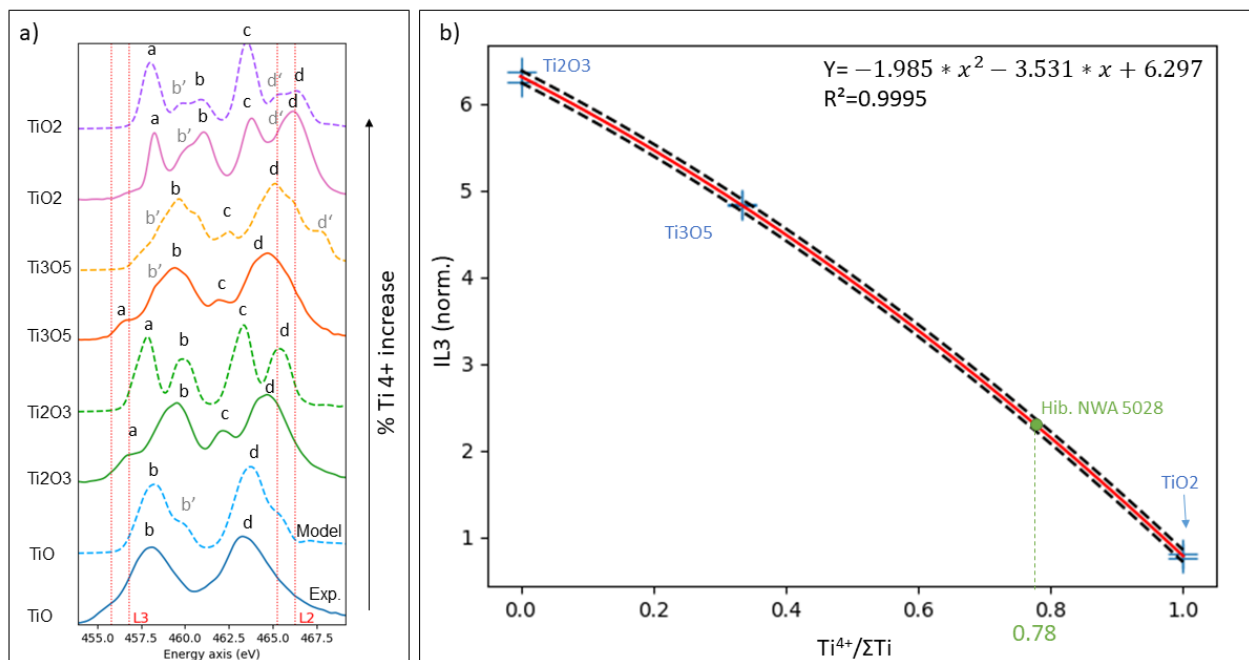
**Figure 1.** Figure 1: a) Ti L2,3 ELNES spectra of the oxide standards (full lines) compared to TELNES 3 simulations (dashed lines). White line integration windows defined by [13] are indicated in red. b) IL3 intensity plotted as a function of the Ti oxidation state for the same standards shown in a). The two crosses for each standard correspond to two separate acquisitions within the grains at different crystal orientation. The mean value obtained for NWA 5028 hibonite is indicated in green.

References

[**1**]     **S. Yoneda and L. Grossman**, **1995**, *Geochim. Cosmochim. Acta*, vol. 59, no. 16, pp. 3413–3444.

[**2**]     **H. Curien, C. Guillemin, J. T. Orcel, and M. Sternberg**, **1956**, *Comptes Rendus Hebd. des Seances l'Academie des Sci.*, vol. 242, no. 24, pp. 2845–2847.

[**3**]     **V. Bermanec, D. Holtstam, D. Sturman, A. J. Criddle, M. E. Back, and S. Šćavničar**, **1996**, *Can. Mineral.*, vol. 34, no. 6, pp. 1287–1297.

[**4**]     **K. Keil and L. H. Fuchs**, **1971**, *Earth Planet. Sci. Lett.*, vol. 12, no. 2, pp. 184–190.

[**5**]     **G. J. Macpherson and L. Grossman**, **1984**, *Geochim. Cosmochim. Acta*, vol. 48, no. 1, pp. 29–46.

[**6**]     **J. R. Beckett, D. Live, F. D. Tsay, L. Grossman, and E. Stolper**, **1988**, *Geochim. Cosmochim. Acta*, vol. 52, no. 6, pp. 1479–1495.

[**7**]     **P. M. Doyle, A. J. Berry, P. F. Schofield, and J. F. W. Mosselmans**, **2016**, *Geochim. Cosmochim. Acta*, vol. 187, pp. 294–310.

[**8**]     **A. J. Berry *et al.***, **2017**, *Chem. Geol.*, vol. 466, pp. 32–40.

[**9**]     **A. Asaduzzaman, K. Muralidharan, and T. J. Zega**, **2021**, *ACS Earth Sp. Chem.*, p. acsearthspacechem.0c00309.

[**10**]    **R. D. Leapman, L. A. Grunes, and P. L. Fejes**, **1982**, *Phys. Rev. B*, vol. 26, no. 2, pp. 614–635.

[**11**]    **L. A. J. Garvie and P. R. Buseck**, **1998**, *Nature*, vol. 396, no. 6712, pp. 667–670.

[**12**]    **P. A. Van Aken, B. Liebscher, and V. J. Styrsa**, **1998**, *Phys. Chem. Miner.*, vol. 25, no. 5, pp. 323–327.

[**13**]     **E. Stoyanov, F. Langenhorst, and G. Steinle-Neumann**, **2007**, *Am. Mineral.*, vol. 92, no. 4, pp. 577–586.

[**14**]     **P. Blaha**, *WIEN2k*, vol. 1. 2019.

[**15**]     **K. Jorissen**, **2007**, *Ph. D. thesis*.

[**16**]     **T. Ramprasad, P. Mane, and T. J. Zega**, in *Lunar and Planetary Science Conference*, 2018, p. 2900.

[**17**]     **F. de la Peña *et al.***, **2020**, *hyperspy/hyperspy: HyperSpy 1.6.0.*

[**18**]     **P. M. Doyle, P. F. Schofield, A. J. Berry, A. M. Walker, and K. S. Knight**, **2014**, *Am. Mineral.*, vol. 99, no. 7, pp. 1369–1382.

[**19**]     **S. B. Simon, A. M. Davis, and L. Grossman**, **1999**, *Geochim. Cosmochim. Acta*, vol. 63, no. 7–8, pp. 1233–1248.